Progress in Organic Coatings 82 (2015) 33–40

Contents lists available at ScienceDirect

Progress in Organic Coatings

journal homepage: www.elsevier.com/locate/porgcoat

Nanocomposite film formations of polyaniline via TiO_2, Ag, and Zn, and their corrosion protection properties

Murat Ates[a,b,*], Erhan Topkaya[a]

[a] Department of Chemistry, Faculty of Arts and Sciences, Namik Kemal University, Degirmenalti Campus, 59030 Tekirdag, Turkey
[b] Department of Chemistry & Biochemistry, University of California Los Angeles, Los Angeles, CA 90095, USA

ARTICLE INFO

Article history:
Received 8 November 2014
Received in revised form 12 January 2015
Accepted 13 January 2015

Keywords:
Corrosion
Nanocomposite
Electrochemical impedance spectroscopy
Polyaniline
Ag-nanoparticle
Zn-nanoparticle

ABSTRACT

Polyaniline (PANI) and its nanocomposites containing TiO_2, Ag, and Zn were electrocoated on an Al1050 electrode by cyclic voltammetry. The modified polymer and the nanocomposite films were characterized by cyclic voltammetry (CV), ultraviolet–visible spectrophotometry (UV–vis), Fourier-transform infrared spectroscopy-attenuated total reflectance (FTIR-ATR), scanning electron microscopy (SEM), energy-dispersion X-ray analysis (EDX), optical microscopy and electrochemical impedance spectroscopic (EIS) methods. The corrosion behavior of the PANI, PANI/TiO_2, PANI/Ag and PANI/Zn nanocomposite films on an Al1050 electrode was studied in a 3.5% NaCl solution. The comparison results were obtained by applying Tafel extrapolation and EIS techniques. The findings indicate that PANI/Ag nanocomposite films yielded higher protection efficiency (PE = 97.54%) compared to PANI (PE = 91.41%), PANI/TiO_2 (PE = 91.91%), and PANI/Zn (PE = 92.52%) nanocomposite films. The results show that the addition of nano-materials (TiO_2, Ag and Zn) into the polymer matrix of PANI enhanced the electrical conductivity of the PANI/Zn film and the corrosion resistance of the polyaniline polymer. These findings were further confirmed by decreasing the oxygen and water permeability and increasing coating adhesion in the presence of TiO_2, Ag and Zn nanomaterials in the PANI. The EIS measurements indicated that the incorporation of TiO_2, Ag, and Zn into the coating increased both the charge transfer and pore resistance.

1. Introduction

Conducting polymers such as polyaniline (PANI), polypyrrole (PPy) or polythiophene (PTh) are used in industrial applications such as rechargeable batteries [1], sensors [2], and corrosion protection [3–5]. Polyaniline (PANI) is a conducting polymer that has been widely studied, as it is believed that it has potential for electronic and optical applications due to its simple and reversible doping/dedoping chemistry, which enables control of several properties, such as electrical conductivity, free-volume and optical activity [6,7]. The charges stored in the polymer layer can be irreversibly consumed during the system's redox reactions, and the ability of the corrosion protection with PANI may be lost over time [8].

To date, many studies in this field have been conducted, with the focus on the synthesis of PANI nanocomposites and their corrosion protection performance [9–12]. The electronic, optical, photo-electrochemical, photo-conductivity, photo-voltaic, thermal, sensing and corrosion protection properties of PANI could be improved by combining it with single-walled nanotubes, multi-walled nanotubes, montmorillonite, graphite, TiO_2, and SiO_2 nanoparticles [13,14]. PANI nanocomposites possess unique mechanical, electrical and structural properties due to the combined effect and the close incorporation between PANI and inorganic and organic compounds at the molecular and atomic levels [15].

Aluminum electrodes have some advantages, including their use as alloys in industrial applications. Aluminum undergoes some corrosion, especially in the presence of chloride ions in the medium. To protect aluminum against corrosion, many methods have been considered, such as chromating, phosphating and using organic inhibitors in the processes. However, these methods are expensive, damaging to the material and difficult to employ due to their toxicity. Therefore, electrocoating aluminum with nanocomposite films as a means of preventing corrosion is more effective than the aforementioned methods.

This work, to the author' knowledge, demonstrates the first attempt to synthesizes polyaniline and its nanocomposites with

* Corresponding author at: Department of Chemistry, Faculty of Arts and Sciences, Namik Kemal University, Degirmenalti Campus, 59030 Tekirdag, Turkey.
Tel.: +90 282 250 2607; fax: +90 282 250 9925.
E-mail addresses: mates@nku.edu.tr, mates@ucla.edu (M. Ates).
URL: http://www.atespolymer.org (M. Ates).

http://dx.doi.org/10.1016/j.porgcoat.2015.01.014
0300-9440/

TiO_2, Ag and Zn by the CV method on an Al1050 electrode. Corrosion performances of the coatings deposited from 0.5 M H_2SO_4 aqueous solution were examined in a 3.5% NaCl corrosive test solution.

2. Materials and methods

2.1. Chemicals

Aniline ((ANI) ≥ 99.5%), sulfuric acid (H_2SO_4, 95–97%), titanium (IV) oxide ((TiO_2) ≥ 99.5%), silver (Ag) nanopowder (particle size < 100 nm), zinc (Zn) nanopowder (particle size < 50 nm) and poly(vinyl pyrrolidone) (PVP) were obtained from Sigma Aldrich, Germany. PVP was used as a dispersant. Acetonitrile ((CH_3CN) ≥ 99.9%), and sodium chloride (NaCl) were obtained from Sigma Aldrich. Nitric acid ((HNO_3) 65%, Sigma Aldrich, Germany), and sodium hydroxide ((NaOH) Sigma Aldrich, Germany) were used in the aluminum sample preparation steps to neutralize the metal surfaces. Ethanol ((C_2H_5OH) ≥ 99.8%, methanol (CH_3OH) Sigma Aldrich, Germany) and distilled water (Purelab Option) solvents were used to clean the Al1050 surface. Corrosion tests were carried out in 3.5% sodium chloride (NaCl) (Sigma Aldrich, Germany) solution. Alumina polishing suspension (0.05 CB micron Gamma Type, CR85S) was obtained from Balkowski International. All chemicals were high grade reagents and used as received.

2.2. Instrumentation

Ivium vertex Potentiostat/Galvanostat (Ivium Technologies) was used for electrochemical coating experiments. The modified electrodes were characterized by SEM-EDX (Leo 1430 VP Make Carl Zeiss) and FTIR Spectrum (Perkin Elmer Spectrum One B) analyses. Ultrasonic bath (Elma), distilled water (Elga DV25), dryer (Memmert), magnetic stirrer (Heidolph MRHei-std), optical microscopy (Best scope) and sensitive balance (Precisa XB 620M) were used in various steps performed during the experiments.

2.3. Aluminum samples

All aluminum samples were obtained from ASM Elexol Aluminum company (Istanbul, Turkey). The surface area of the Al1050 samples was prepared as 2.0 cm^2. The atomic composition of the Al1050 samples was as follows: 99.58% Al, 0.30% Fe, 0.09% Si, 0.02% Mn, and 0.01% Cu.

2.4. Preparing and cleaning of aluminum samples

Prior to experiment, the working electrode was polished with a sequence of emery papers of different grades (1000, 1200 and 2000), and the surfaces of the aluminum samples were cleaned by acidic and basic solutions, as well as washed by alcoholic solvents and water. The samples were immersed into a 5% NaOH solution for 3 min and washed with an ethanol solution. Then, they were immersed into a concentrated nitric acid (65%) solution for neutralization. Ultrasonication with distilled water was used to remove the contaminants.

2.5. Electropolymerization processes

Cyclic voltammetry was performed using IviumStat (Ivium Technologies, the Netherlands) (Software: Iviumsoft and Faraday cage: BASI cell stand C3) in a three-electrode configuration, which employs Al1050 as the working electrode, platinum wire as the counter electrode, and Ag/AgCl as the reference electrode. The working electrode was carefully polished with alumina slurry and cleaned in an ultrasonic bath before each experiment.

Electrochemical impedance spectroscopy (EIS) measurements were performed in a monomer-free electrolyte solution with the perturbation amplitude of 10 mV on the Al1050 electrode over the frequency range of 10 mHz to 100 kHz with the IviumStat potansiostat/galvanostat. Open circuit potential was used in all experiments and modified polymer films were allowed to equilibrate for 10 min at each potential before the measurements [16].

3. Results and discussions

3.1. Electrochemical synthesis of PANI, PANI/TiO_2, PANI/Ag and PANI/Zn films

Aniline (ANI), ANI/TiO_2, ANI/Ag and ANI/Zn nanocomposites were electrochemically synthesized on Al1050 electrodes in 0.5 M H_2SO_4 solution by the CV method. Polymerization conditions were taken in the potential range between −0.2 V and +0.8 V at a scan rate of 50 mV s^{-1} for 8 cycles. The electropolymerization of ANI, ANI/TiO_2, ANI/Ag and ANI/Zn is given in Fig. 1.

The initial ANI concentration for all measurements was 0.4 M. The electrogrowth of ANI and nanocomposites indicates that upon repeated scans, new redox processes appeared at lower potentials (E_a = 0.09 V for ANI, E_a = 0.03 V for ANI/TiO_2, E_a = 0.15 V for ANI/Ag and E_a = 0.08 V for ANI/Zn), indicating the formation of an electroactive polymer film. CV application results in the formation of radical cations by the release of electrons from the monomer. Generated electroactive monomers form dimers and transform into oligomers by releasing hydrogen ions. The dimers are subsequently oxidized again and coupled with another oxidized segments. Finally, the PANI and PANI/TiO_2, PANI/Ag and PANI/Zn nanocomposite films were formed on the Al1050 electrode [17].

Table 1 summarizes the anodic (E_a) and cathodic peak potentials (E_c), their difference ($\Delta E = |E_a - E_c|$), the anodic current (i_a), cathodic current (i_c) and the anodic and cathodic current ratio (i_a/i_c). ANI, ANI/TiO_2, ANI/Ag and ANI/Zn show the reversible redox behaviors. The reversible CV was obtained by two criteria: $i_a/i_c \approx 1$, $\Delta E \leq 0.59$ V. The CV results showed that ANI/Ag has different oxidation and reduction potentials, the lowest separation between the anodic and cathodic peaks (ΔE = 0.01) and the highest anodic and cathodic current ratio (i_a/i_c = 0.95). As a result, the highest reversible redox behaviors were observed for the ANI/Ag film. ΔE is associated with the ion transport resistance involved in these redox reactions [18,19].

As a result, ANI and its nanocomposites with TiO_2, Ag and Zn were successfully electrocoated on the Al1050 substrates. All CV results show that reversible redox behaviors were obtained by the CV method.

3.2. SEM-EDX analysis

The surface morphologies of an uncoated Al1050 electrode and the electrochemically synthesized PANI, PANI/TiO_2, PANI/Ag and PANI/Zn nanocomposite films were studied using scanning electron microscopy (SEM-EDX) as shown in Fig. 2a–e. PANI and nanocomposite films of PANI, PANI/TiO_2, PANI/Ag and PANI/Zn were successfully obtained on the Al1050 substrate. SEM samples

Table 1
Redox parameters of electrogrowth of ANI, ANI/TiO_2, ANI/Ag and ANI/Zn were obtained from CV.

Materials	E_a/V	E_c/V	($\Delta E = \|E_a - E_c\|$)	i_a/mA	i_c/mA	i_a/i_c
ANI	0.09	−0.13	0.04	7.99	8.79	0.90
ANI/TiO_2	0.03	−0.25	0.22	4.25	3.99	1.06
ANI/Ag	0.15	−0.14	0.01	14.2	14.9	0.95
ANI/Zn	0.08	−0.20	0.12	4.83	4.60	1.05

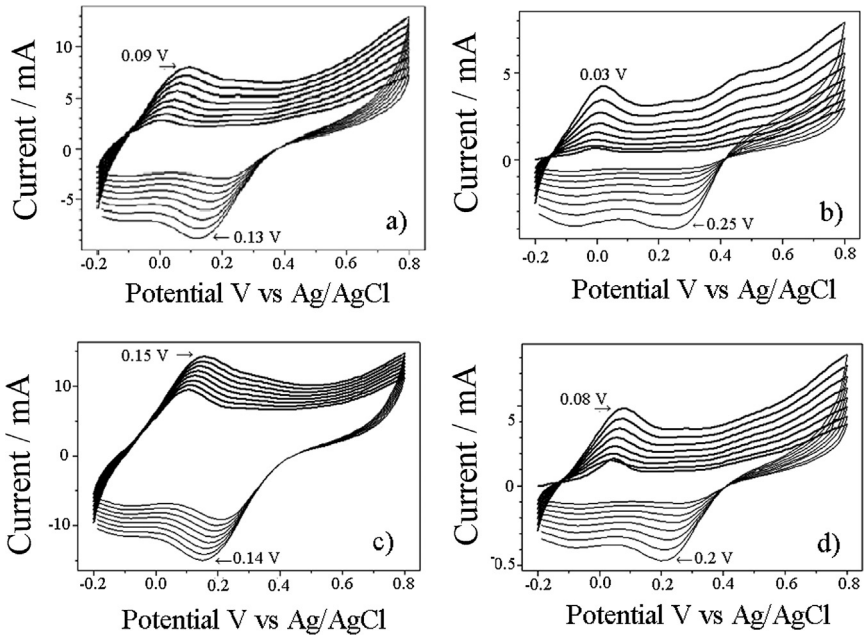

Fig. 1. (a) ANI electropolymerized on the Al1050 electrode by CV: (b) ANI/TiO_2 electropolymerized on the Al1050 electrode by CV: (c) ANI/Ag electropolymerized on the Al1050 electrode by CV: (d) ANI/Zn electropolymerized on the Al1050 electrode by CV. The experimental conditions were the same for all samples. The 0.5 M H_2SO_4 solution was used and the potential ranged from −0.2 V to +0.8 V, with the scan rate of 50 mV s^{-1} at 8 cycles $[ANI]_0$ = 0.4 M. TiO_2, Ag and Zn were taken as 1% (0.85 mg) in the total composition.

were prepared in the same electrodeposition conditions. Electrogrowth of ANI and the nanocomposites was performed in the potential range between −0.2 V and +0.8 V and at a scan rate of 50 mV s^{-1} in a 0.5 M H_2SO_4 solution for 8 cycles.

A SEM image of the uncoated Al1050 electrode is shown in Fig. 2a. In addition, the PANI film displayed granular structure (Fig. 2b). A solution of 1% TiO_2 nanoparticles was added to the nanocomposite monomer solution. Grain structures were also observed for the PANI/TiO_2 film (Fig. 2c). A homogeneous coating of PANI/Ag confirms a homogeneous coating on the Al1050 substrate (Fig. 2d). The highest reversible CV was obtained for the PANI/Ag nanocomposite film, which also displayed the most homogeneous film formation. Furthermore, these results are supported by the highest protection efficiency of the PANI/Ag nanocomposite film, as PE = 97.5%. A SEM image of the PANI/Zn nanocomposite film also shows the grain structure on the Al1050 electrode (Fig. 2e). Moreover, a close relationship between the film morphology obtained from the SEM images and the protection efficiency is evident. SEM analyses show that PANI, PANI/TiO_2 and PANI/Zn nanocomposite films have granular structure. Their protection efficiency was obtained as PE = 91.41%, 91.91% and 92.52%, respectively.

The EDX results show that weight percentages of the elements in polymer and nanocomposite matrix were successfully obtained, as shown in Table 2. There is a noticeable difference among the PANI and PANI/TiO_2, PANI/Ag and PANI/Zn nanocomposite films, indicating the weight percentage of the electrochemically obtained films of C element (27.18%, 31.07%, 11.22% and 25.20% for PANI, PANI/TiO_2, PANI/Ag and PANI/Zn nanocomposite films, respectively). The lowest C (11.22%), S (6.88%) and O (10.10%) were obtained for PANI/Ag nanocomposite films. However, the highest Ag percentage (8.28%) was obtained for PANI/Ag nanocomposite film. The other nanomaterials were obtained as 1.72% for PANI/TiO_2 and 1.62% for PANI/Zn nanocomposite materials. In addition, the weight percentage of N for the PANI film was obtained as 15.52% [20]. Nanomaterials in the polymer matrix – such as TiO_2, SiC, Fe_2O_3 etc – significantly increase the corrosion protection capability [21].

3.3. UV–vis spectroscopy

The UV–vis spectrophotometry measurements of PANI, PANI/TiO_2, PANI/Ag and PANI/Zn were taken in 0.01 g/L DMF solvent as shown in Fig. 3a–d. The characteristic peaks of PANI were obtained at 348 nm, 487 nm and 582 nm. The peak at 348 nm corresponds to the π–π^* transition of PANI. In addition, the peak at 582 nm refers to n–π^* transition of quinine-imine PANI groups [22].

PANI/TiO_2 nanocomposite was measured in the same experimental conditions as those depicted in Fig. 3b. The peak at 317 nm shifts due to the introduction of the TiO_2 nanomaterials into the polymer matrix. There is a π–π^* transition between conjugated polymer chains and TiO_2 nanomaterials [23,24]. The peak at 361 nm shows the n–π^* transition of PANI/TiO_2 nanocomposite films.

The UV–vis spectrum of PANI/Ag is given in Fig. 3c where peaks at 380 nm, 401 nm, and 426 nm are visible. In general, Ag

Table 2
EDX analysis of PANI, PANI/TiO_2, PANI/Ag and PANI/Zn nanocomposite films.

Elements	Weight/%							
	Al	S	O	N	C	Ti	Ag	Zn
Uncoated Al1050	100	–	–	–	–	–	–	–
PANI	4.96	13.45	38.89	15.52	27.18	–	–	––
PANI/TiO_2	0.26	13.63	42.05	11.27	31.07	1.72	–	–
PANI/Ag	36.55	6.88	26.88	10.19	11.22	––	8.28	–
PANI/Zn	0.19	14.63	43.76	14.60	25.20	–	–	1.62

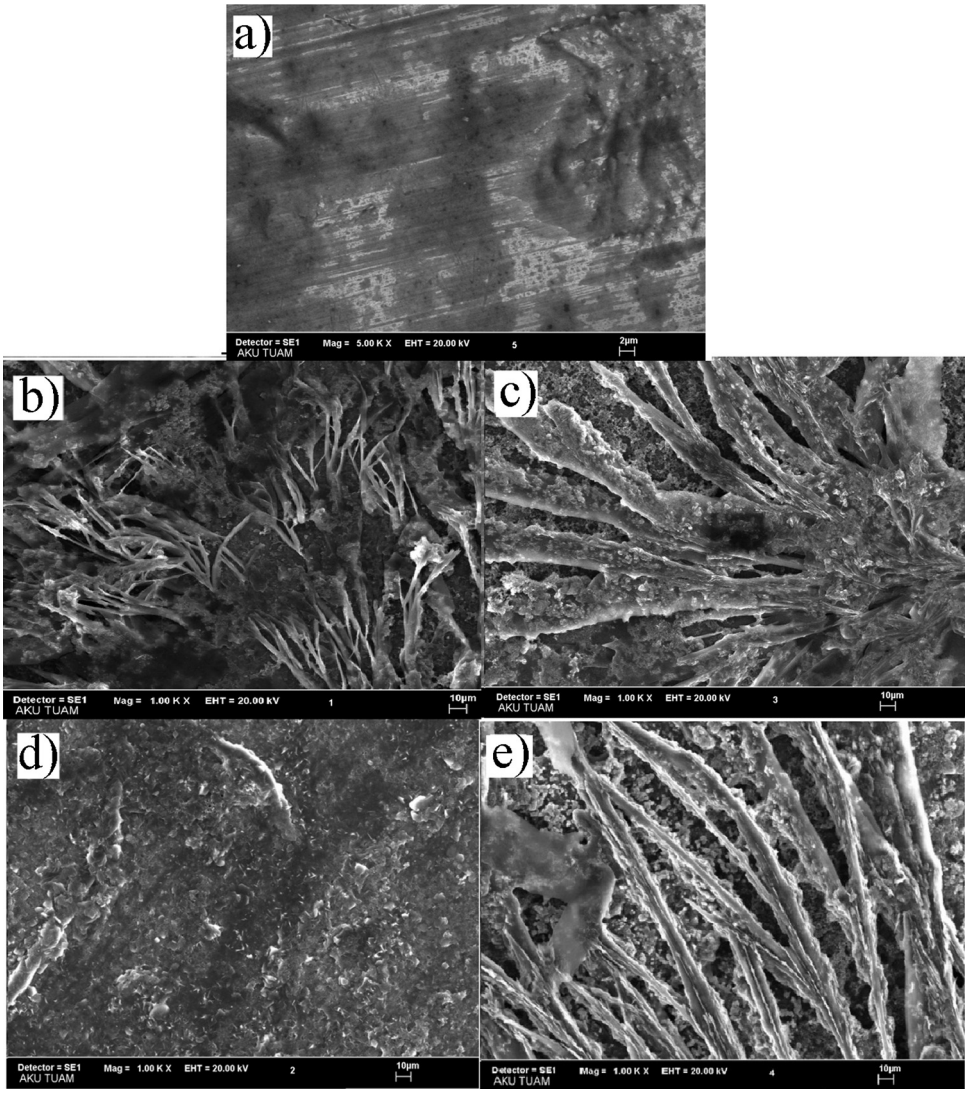

Fig. 2. SEM images of (a) uncoated Al1050 electrode, (b) PANI on Al1050, (c) PANI/TiO_2 on Al1050, (d) PANI/Ag on Al1050, and (e) PANI/Zn on Al1050. The SEM images of all samples were taken under the same conditions. The 0.5 M H_2SO_4 was used and the potential ranged from −0.2 V to +0.8 V. The scan rate of 50 mV s^{-1} at 8 cycles and $[ANI]_0$ = 0.4 M were used. TiO_2, Ag and Zn were taken as 1% (0.85 mg) in the total composition.

nanoparticles were defined in the UV–vis spectrum at the 400–450 nm wavelengths. The peak at 426 nm was identified as arising from the Ag nanomaterials, based on the findings reported in the extant literature [25]. This peak also refers to π–π* transition of PANI, which is due to the existence of Ag nanoparticles [26].

PANI/Zn nanocomposite measurements were taken in the same experimental conditions as those shown in Fig. 3d. The peak at 348 nm and those in the 487–582 nm range belong to π–π* transition in the benzonoid cycle for PANI [27]. The peak difference between the PANI and PANI/Zn nanocomposite was caused by the

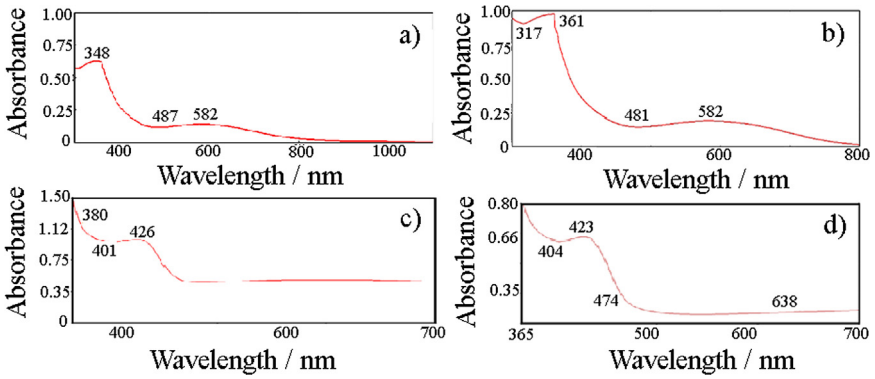

Fig. 3. UV–vis spectra of (a) PANI on Al1050, (b) PANI/TiO_2 on Al1050, (c) PANI/Ag on Al1050, (d) PANI/Zn on Al1050. The UV–vis spectra were obtained in 0.01 g/L DMF solution.

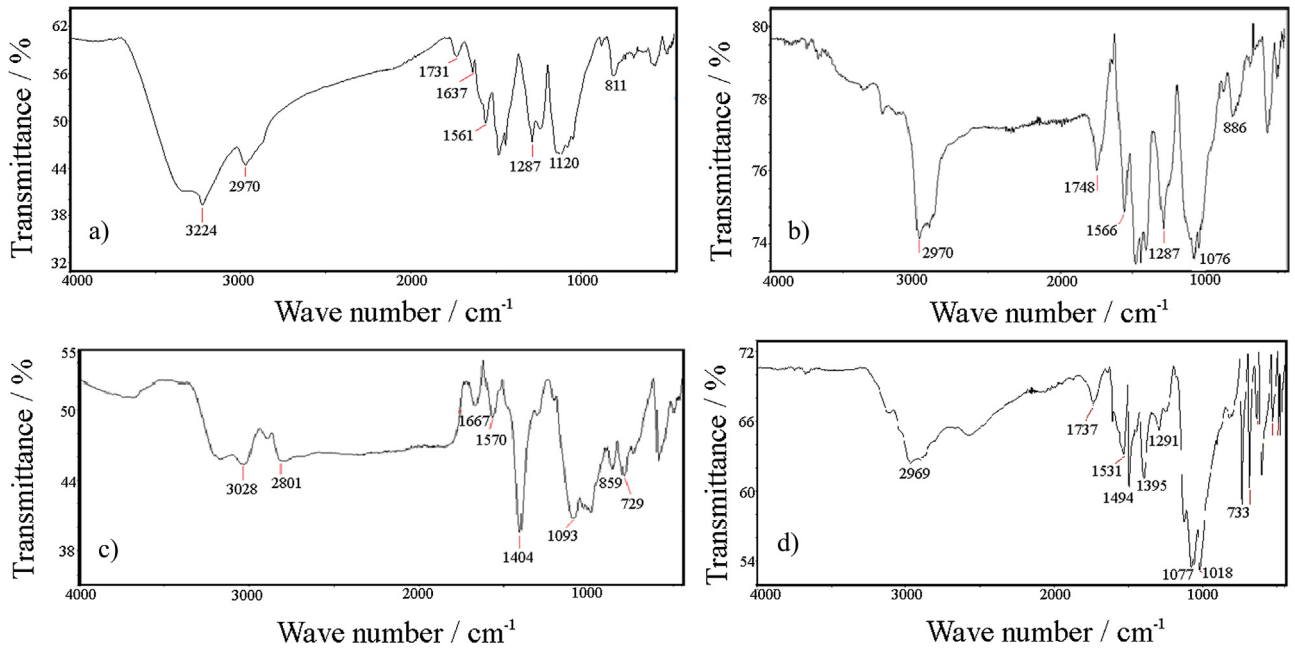

Fig. 4. FTIR-ATR images of (a) PANI on Al1050, (b) PANI/TiO_2 on Al1050, (c) PANI/Ag on Al1050, and (d) PANI/Zn on Al1050.

Zn nanoparticles. The change of nanomaterials (Ag, TiO_2, and Zn) also resulted in different absorbance of the materials at 404, 423, 474 and 638 nm. Therefore, different π–π^* transition peaks pertaining to PANI and PANI nanomaterials could be deduced from their corresponding UV–vis spectra.

3.4. FTIR-ATR analysis

The FTIR-ATR spectra pertaining to the electrocoated PANI, PANI/TiO_2, PANI/Ag and PANI/Zn-nanoparticles on Al1050 electrodes are given in Fig. 4. The peaks in the 3224–2970 cm^{-1} range are attributed to C—H stretching, while those at about 1561 cm^{-1} indicate aromatic stretching of the double C=C bond. The peaks at 1731–1241 cm^{-1} are likely due to C—O stretching. The intense band located at 1287 cm^{-1} is attributed to C—N bond of secondary aromatic amine structure, while the peaks at 564–490 cm^{-1} indicate the ferrite structure. The additional peaks are caused by introducing peak shifts, where the chain regulations are obtained into the polymer matrix [28–30] (Fig. 4a).

The FTIR-ATR spectrum of PANI/TiO_2 films on Al1050 electrodes is given in Fig. 4b. The peak at 1076 cm^{-1} refers to the Ti—O—C structure and that at 1287 cm^{-1} corresponds to the C—N structure of the benzoid cycle. The peaks at 2970 cm^{-1}, 1566–1481 cm^{-1} and 886 cm^{-1} are attributed to C—H stretching, C=C stretching of the benzoid cycle, and C—H out of bending of benzene cycle, respectively.

The FTIR-ATR spectrum of PANI/Ag films on an Al1050 electrode is given in Fig. 4c. The peaks at 1300 cm^{-1}, 1404 cm^{-1}, 1093 cm^{-1} and 859 cm^{-1} are attributed to the PANI film. The peak at 859 cm^{-1} refers to a C—H bond of a π-substituted benzene cycle. The peaks at 1404 and 1570 cm^{-1} show the N—B—N and N=Q=N of the benzoid and quinoid of the PANI structure. The peaks at 1093 and 1300 cm^{-1} refer to the C—N bonds.

The FTIR-ATR spectrum of PANI/Zn films on Al1050 electrodes is given in Fig. 4d. The characteristic vibration frequencies of Zn nanoparticles were obtained as 530, 636, 733 and 2969 cm^{-1}, while the defined peaks were obtained at 1077, 1291, 1494 and 1531 cm^{-1}. These peaks were also obtained for the PANI film. The peaks at 1494 and 1531 cm^{-1} refer to the benzonoid and quinoid cycle of C=C vibration frequencies, respectively. The peak at 1291 cm^{-1} refers to the C=C strain, while the peak at 1077 cm^{-1} is attributed to C—H bending vibration [31]. It can be concluded that combining PANI with TiO_2, Ag and Zn nanoparticles enhance the protection properties of the electrocoating matrix.

3.5. Electrochemical impedance spectroscopy

Electrochemical impedance spectroscopy is a powerful technique that can yield valuable information on the capacitor behavior of modified electrodes. In this work, all the impedance spectra were measured at the corresponding open circuit potential. The low frequency capacitance values (C_{LF}) from a Nyquist plot were obtained from the slope of a plot of the imaginary component (Z'') of the impedance at low frequencies versus the inverse of the reciprocal frequency (f), where $\pi = 3.14$, $f = 0.01$ Hz and Z'' is the imaginary impedance using the equation given as [32];

$$C_{LF} = -1/2\pi \times f \times Z''$$

The C_{LF} values were obtained for PANI, PANI/TiO_2, PANI/Ag, and PANI/Zn nanoparticle films from their respective Nyquist plots (Fig. 5a). The results show that the lowest C_{LF} value was obtained for the PANI/Ag film ($C_{LF} = 0.78$ F cm^{-2}), while the highest C_{LF} was obtained for the PANI/TiO_2 film ($C_{LF} = 60.76$ F cm^{-2}). The other C_{LF} values were 39.61 and 54.16 F cm^{-2}, for the PANI/Zn and PANI films, respectively. Thus, as different C_{LF} values for different nanocomposite films were measured, we can claim that C_{LF} values confirm the sensitivity and successful synthesis of nanocomposite films.

A Bode-magnitude plot gives the extrapolation line to the log$Z$ axis at $w = 1$ ($\log w = 0$) yielding the value of C_{dl} from the following equation. IZI = $1/C_{dl}$ [33] (Fig. 5b). The obtained C_{dl} values are: $C_{dl} = 0.19$ mF cm^{-2} for the PANI films, $C_{dl} = 0.08$ mF cm^{-2} for the PANI/TiO_2, $C_{dl} = 0.07$ mF cm^{-2} for the PANI/Ag, and $C_{dl} = 0.14$ mF cm^{-2} for the PANI/Zn films. Obtaining different C_{dl} values for different nanocomposite films in the Helmholtz plane shows that using different AC frequencies produces different impedance values for the studied nanocomposite films and double layers in the solution.

Bode-phase plots of the uncoated Al1050, as well as PANI/Ag, PANI/TiO_2, PANI/Zn, and PANI films were given with respect

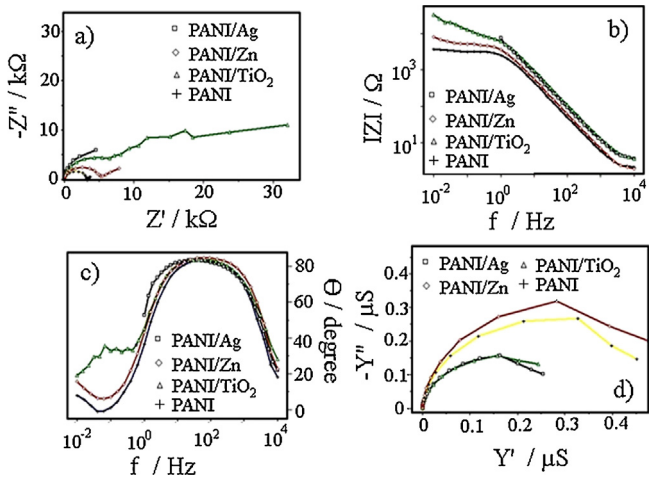

Fig. 5. EIS graphs of PANI, PANI/TiO_2, PANI/Ag, and PANI/Zn nanoparticles on an Al1050 electrode, with (a) Nyquist, (b) Bode-magnitude, (c) Bode-phase, and (d) Admittance plots. Polymerization was obtained by the CV method.

Table 3
The EIS results of electrochemically synthesized PANI, PANI/TiO_2, PANI/Ag, and PANI/Zn coated Al1050 electrodes.

Material	EIS results	Time/days				
		1st	2nd	3rt	7th	14th
PANI	C_{LF}/F cm^{-2}	54.16	39.22	41.46	122.48	122.12
	C_{dl}/mF cm^{-2}	0.19	0.13	0.18	0.08	0.14
	θ/degree	83.32	82.51	80.30	81.16	83.52
PANI/TiO_2	C_{LF}/F cm^{-2}	60.76	57.27	96.22	139.68	248.81
	C_{dl}/mF cm^{-2}	0.08	0.15	0.067	0.06	0.07
	θ/degree	83.79	80.60	83.90	81.54	83.90
PANI/Ag	C_{LF}/F cm^{-2}	0.78	4.98	0.048	2.17	1.03
	C_{dl}/mF cm^{-2}	0.07	0.08	0.26	0.04	0.070
	θ/degree	83.56	59.88	83.60	77.71	80.14
PANI/Zn	C_{LF}/F cm^{-2}	39.61	46.29	65.26	104.14	90.47
	C_{dl}/mF cm^{-2}	0.14	0.17	0.13	0.06	0.08
	θ/degree	84.83	81.60	81.78	81.07	80.01

to changing log (f) values (Fig. 5c). The imaginary part of the impedance spectra at low frequencies represents the capacitive behavior of the electrode, while the 90° vertical line corresponds to an ideal capacitor [34]. The highest phase angle was obtained as θ = ~84.83° for the PANI/Ag, PANI/TiO_2, PANI/Zn, and PANI films. As can be seen, a decrease in frequency results in a decrease in phase angle. An admittance plot was obtained for the PANI, PANI/TiO_2, PANI/Ag, and PANI/Zn nanocomposite films in a 0.5 M H_2SO_4 solution as given in Fig. 5d. The highest conductivity value was obtained for the PANI/Zn film at Y' = ~300 mS. The conductivity of other films was the following order: PANI > PANI/TiO_2 > PANI/Ag at Y' = ~150 mS. In addition, the conductivity values of PANI/Ag and PANI/TiO_2 nanocomposite films were found to be similar.

The EIS results of C_{LF}, C_{dl} and θ of PANI, PANI/TiO_2, PANI/Ag and PANI/Zn nanocomposites are given in Table 3. The EIS results indicate that these films exhibit a time-dependent behavior, whereby, after the first 7 days, the C_{sp}, C_{dl} and θ values significantly increased. This finding suggest that the modified electrodes are stable for 7 days only. The Nyquist plots of the PANI, PANI/TiO_2, PANI/Ag and PANI/Zn nanocomposite films clearly reveal that all examined films offer greater resistance to corrosion during the 7 days of immersion due to the higher impedance compared to an uncoated Al1050 electrode. The increase in the impedance values pertaining to the PANI, PANI/TiO_2, PANI/Ag and PANI/Zn nanocomposite films can be attributed to the establishment of the passive layer on the metal surface over time, which is due to the oxidizing property

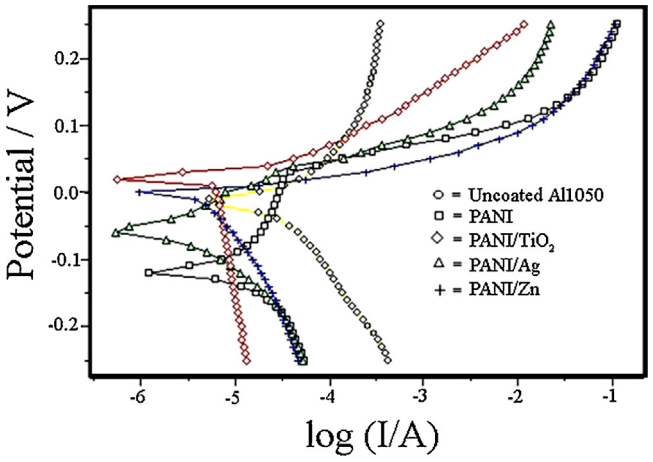

Fig. 6. Tafel extrapolation plot of an uncoated Al1050 electrode, PANI, PANI/TiO_2, PANI/Ag and PANI/Zn on an Al1050 electrode.

of the conducting polymers [35]. Therefore, in agreement with the polarization curves, PANI/Ag nanocomposite films have the best protection efficiency compared to the other films.

3.6. Corrosion protection abilities of coated electrodes

The anti-corrosive properties of the uncoated Al1050, PANI, PANI/TiO_2, PANI/Ag and PANI/Zn films were evaluated in a 3.5% NaCl solution with the potentiodynamic polarization curves (Fig. 6). It has been previously shown that conductive polymers could provide protection to the metal layer because of their protection ability [36].

The corrosion parameters, such as corrosion potential (E_{cor}), corrosion current (i_{cor}), Tafel constants (β_a and β_c), polarization resistance (R_p), protection efficiency (PE), corrosion rate (CR) and porosite (P), are listed in Table 4. The corrosion potential value (E_{corr}) pertaining to the uncoated Al1050 electrode is observed to be −0.081 V. The corrosion current density (i_{corr}) values of all coated electrodes were significantly lower than that of the uncoated Al1050 electrode, indicating that polymer coating with and without nanoparticles provides corrosion protection to the Al1050 electrode.

Corrosion parameters were obtained from the Tafel extrapolation plot, as shown in Fig. 6. Corrosion current density (i_{cor}) was measured as 32.5 μA cm^{-2} for the uncoated Al1050 electrode, while it decreased after the coating processes. Thus, i_{cor} values were measured as i = 2.79 μA cm^{-2} for PANI, i = 2.43 μA cm^{-2} for PANI/Zn, i = 2.63 μA cm^{-2} for PANI/TiO_2, and 0.80 μA cm^{-2} for PANI/Ag synthesized electrochemically. Protection efficiency (PE/%) was obtained by using the following expression:

$$\mathrm{PE} = \frac{(i^\circ - i)}{i^\circ} \times 100$$

where i° is the current density of an uncoated film, and i is the current density of a coated film. PE was obtained as 91.41%, 92.52%, 91.91% and 97.54% for PANI, PANI/Zn, PANI/TiO_2 and PANI/Ag, respectively. Corrosion rate (CR/mm y^{-1}) was obtained using the expression:

$$C_{\mathrm{corr}} = \frac{[0.13 \times i_{\mathrm{corr}}(\mathrm{EW})]}{(Ad)},$$

where EW denotes the equivalent weight (g/eq), A represents area (cm^{-2}) and d is density (g/cm^3). Corrosion resistance was calculated using the expression:

$$R_{\mathrm{corr}} = 0.0032 \times i_{\mathrm{corr}} \times M \times n \times d,$$

Table 4
Tafel extrapolation plot results of uncoated Al1050, PANI, PANI/TiO_2, PANI/Ag and PANI/Zn.

Material	E_{cor}/V	i_{cor} (μA/cm^2)	β_a (V/dec)	β_c (V/dec)	CR/mm y^{-1}	R_p/Ω	PE/%	P
Al1050	−0.081	32.5	0.408	0.211	0.354	927.6	–	–
PANI	−0.117	2.79	0.191	0.071	0.030	4035	91.41	0.187
PANI/Zn	0.001	2.43	0.018	0.203	0.026	1454	92.52	0.403
PANI/TiO_2	0.017	2.63	0.037	0.229	0.078	2622	91.91	0.204
PANI/Ag	−0.052	0.80	0.067	0.078	0.009	9825	97.54	0.080

where i_{corr} denotes corrosion current density, M is molar mass (g/mol), n is charge number, and d is the density of the tested metal (g/cm^3). Polarization resistance (R_p) was obtained from the Stern-Geary formula:

$$R_p = (\beta_a \times \beta_b)/2.303 \times I_{corr}(\beta_a + \beta_c),$$

where I_{corr} represents corrosion current density, β_a denotes the Tafel slope of the anode, and β_c is the Tafel slope of the cathode. Corrosion rate of the uncoated Al1050 electrode was obtained as CR = 0.354 mm y^{-1}. The lowest CR was obtained for the PANI/Ag nanocomposite film (CR = 0.009 mm y^{-1}). The calculated PE was 40.71 times higher than that of the uncoated Al1050 electrode. The highest value of the PE (97.54%) was found for the PANI/Ag nanocomposite film. In the pertinent literature, the protection mechanism of conducting polymers is still debated. Thus far, four main mechanisms have been reported to explain the processes during corrosion tests [37]: (a) anodic protection, (b) displacement of the electrochemical interface, (c) barrier effect and (d) self-healing properties. Anodic protection of PANI, PANI/TiO_2, PANI/Ag and PANI/Zn nanocomposite films and barrier effects were found to contribute to high protective performances.

The porosity (P) values were obtained as P = 0.187, 0.403, 0.204 and 0.080 for PANI, PANI/Zn, PANI/TiO_2, and PANI/Ag, respectively. The lowest porosity (P = 0.080) was obtained for the PANI/Ag nanocomposite film which also displayed the highest protection efficiency (PE = 97.54%).

4. Conclusions

In this study, PANI, PANI/Zn, PANI/TiO_2 and PANI/Ag-nanocomposite coatings were electropolymerized on an Al1050 substrate in a 0.5 M H_2SO_4 aqueous solution containing 0.4 M aniline and 1% nanoparticles under ultrasonic irradiation. The CV method was successfully employed for the preparation of TiO_2, Ag and Zn nanoparticles in the presence of PANI. The modified electrodes were characterized by FTIR-ATR, SEM-EDX, EIS, and Tafel extrapolation methods. PANI, PANI/Zn, PANI/TiO_2 and PANI/Ag-nanocomposites on Al1050 were tested for corrosion protection ability against a 3.5% NaCl solution. The highest protection efficiency was obtained for the PANI/Ag nanocomposite film (PE = 97.54%). Based on the corrosion test results, it can be concluded that the CV, SEM and EIS findings also supported the Tafel extrapolation results and thus confirmed that PANI/Ag nanocomposite films had the highest protective properties. Thus, we posit that PANI/Ag nanocomposite films might be used as protection materials for battery and supercapacitor device applications which are promising power generation technologies.

Author contributions

The manuscript was written through the contributions of all authors. All authors have given approval to the final version of the manuscript.

Acknowledgements

The authors thank Serhat Tikiz (Afyon Kocatepe Univ., TUAM, Afyon, Turkey) for the SEM-EDX measurements and Dr. Argun Gokceoren (ITU, Istanbul, Turkey) for the FTIR-ATR measurements. The financial support from Namik Kemal University, Tekirdag, Turkey, project number: NKUBAP.00.10.AR.12.09 is gratefully acknowledged. The authors also thank ASM Elexol Aluminum Company (Istanbul, Turkey) for providing the Al1050 electrode.

References

[1] N. Balis, V. Dracopoulos, M. Antoniadou, P. Lianos, One step electrodeposition of polypyrrole applied as oxygen reduction electrocatalyst in photo activated fuel cells, Electrochim. Acta 70 (2012) 338–343.
[2] J. Li, H.Q. Xie, Y. Li, Fabrication of gold nano-particles/polypyrrole composite-modified electrode for sensitive hydroxylamine sensor design, J. Solid State Electrochem. 16 (2012) 795–802.
[3] M. Shabani-Nooshabadi, S.M. Ghoreishi, M. Behpour, Direct electrosynthesis of polyaniline-montmorillonite nanocomposite coatings on aluminum alloy 3004 and their corrosion protection performance, Corros. Sci. 53 (2011) 3035–3042.
[4] Y.H. Yu, Y.Y. Lin, C.H. Lin, C.C. Chan, Y.C. Huang, High performance polystyrene/graphene based nanocomposites with excellent anti-corrosion properties, Polym. Chem. 5 (2014) 535–550.
[5] H.G. Wei, D.W. Ding, S.Y. Wei, Z.H. Guo, Anti corrosive conductive polyurethane multiwalled carbon nanotube nanocomposite, J. Mater. Chem. A 1 (2013) 10805–10813.
[6] J. Ryu, C.B. Park, Synthesis of diphenylalanine/polyaniline core/shell conducting nanowires by peptide self-assembly, Angew. Chem. Int. Ed. 48 (2009) 4820–4823.
[7] M. Molberg, D. Crespy, P. Rupper, F. Nuesch, J.A.E. Manson, C. Lowe, D.M. Opris, High breakdown field dielectric elastomer actuators using encapsulated polyaniline as high dielectric constant filler, Adv. Funct. Mater. 20 (2010) 3280–3291.
[8] H. Ashassi-Sorkhabi, R. Bagheri, B. Rezaei-Moghadam, Protective properties of PPy-Au nano-composite coatings prepared by sonoelectrochemistry and optimized by the Taguchi method, J. Appl. Polym. Sci. 131 (2014) 41087–41096.
[9] E. Akbarinezhad, M. Ebrahimi, F. Sharif, A. Ghanbarzadeh, Evaluating protection performance of zinc rich epoxy paints modified with polyaniline and polyaniline-clay nanocomposite, Prog. Org. Coat. 77 (2014) 1299–1308.
[10] M. Shabani-Nooshabadi, S.M. Ghoreishi, Y. Jafari, N. Kashanizadeh, Electrodeposition of polyaniline-montmorillonite nanocomposite coatings on 316L stainless steel for corrosion prevention, J. Polym. Res. 21 (2014) 416–426.
[11] P. Piromruen, S. Kongparakul, P. Prasassarakich, Synthesis of polyaniline/montmorillonite nanocomposites with an enhanced anticorrosive performance, Prog. Org. Coat. 77 (2014) 691–700.
[12] J. Wang, J.O. Iroh, S. Hall, Effect of polyaniline-modified clay on the processing and properties of clay polyimide nanocomposites, Appl. Clay Sci. 99 (2014) 215–219.
[13] A.E.A. Hermas, M.A. Salam, S.S. Al-Juaid, In-situ electrochemical preparation of multi-walled carbon nanotubes/polyaniline composite on the stainless steel, Prog. Org. Coat. 76 (2013) 1810–1813.
[14] Z.A. Hu, Y.L. Xie, Y.X. Wang, L.P. Mo, Y.Y. Yang, Z.Y. Zhang, Polyaniline/SnO_2 nanocomposite for supercapacitor applications, Mater. Chem. Phys. 114 (2009) 990–995.
[15] H. Gomez, M.K. Ram, F. Alvi, E. Stefanakos, A. Kumar, Novel synthesis, characterization, and corrosion inhibition properties of nanodiamond-polyaniline films, J. Phys. Chem. C 114 (2010) 18797–18804.
[16] M. Ates, N. Uludag, T. Karazehir, F. Arican, A novel synthesis of 4-toluene 9H-carbazole-9-carbodithioate, electropolymerization and impedance study, Express Polym. Lett. 8 (2014) 480–490.
[17] A.S. Sarac, M. Ates, E.A. Parlak, E.F. Turcu, Characterization of micrometer-sized thin films of electrocoated carbazole with p-tolylsulfonyl pyrrole on carbon fiber microelectrodes, J. Electrochem. Soc. 154 (2007) D283–D291.
[18] E. Csahok, E. Vieil, G. Inzelt, In situ dc conductivity study of the redox transformations and relaxation of polyaniline films, J. Electroanal. Chem. 482 (2000) 168–177.
[19] K. Rossberg, G. Paasch, L. Dunsch, S. Ludwig, The influence of porosity and the nature of the charge storage capacitance on the impedance behavior of electropolymerized polyaniline films, J. Electroanal. Chem. 443 (1998) 49–62.

[20] K. Ding, Z. Jia, W. Mac, R. Tong, X. Wang, Polyaniline and polyaniline thiokol rubber composite coatings for the corrosion protection of mild steel, Mater. Chem. Phys. 76 (2002) 137–142.
[21] C. Muller, M. Sarnet, M. Benballa, ZnNi/SiC composites obtained from an alkaline bath, Surf. Coat. Technol. 162 (2003) 49–53.
[22] J. Stejskal, D. Hlavata, P. Holler, M. Trchovam, J. Prokes, I. Sapurina, Polyaniline prepared in the presence of various acids: a conductivity study, Polym. Int. 53 (2004) 294–300.
[23] Y. Lu, A. Pich, H.J.P. Adler, G. Wang, D. Rais, S. Nespurek, Composite polypyrrole-containing particles and electrical properties of thin films prepared therefrom, Polymer 49 (2008) 5002–5012.
[24] M.G. Murali, M.G. Ramya, D. Udayakumar, N.B. Lakshmi, R. Philip, Synthesis and third order optical nonlinearity studies of the donor acceptor conjugated polymer, poly(2-[3,4-didodecyloxy-5-(1,3,4-oxadazol-2-yl) thiophen-2-yl)-5-phenyl-1,3,4-oxadiazol) and a polymer/TiO_2 nanocomposite, Synth. Met. 160 (2010) 2520–2525.
[25] S. Nallusamy, J.B. Gopalakrishnan, R.K. Sekar, J.B.B. Rayappan, Spatial variation of local field by the Ag nanoparticle on the PANI matrix: a nonlinear optics (NLO) perspective, J. Appl. Sci. 12 (2012) 1691–1695.
[26] A. Malinauskas, R. Holze, Cyclic UV–vis spectro voltammetry of polyaniline, Synth. Met. 97 (1998) 31–36.
[27] J. Arjomandi, S. Tadayyonfar, Electrochemical synthesis and in-situ spectro-electrochemistry of conducting polymer nanocomposites. I. Polyaniline/TiO_2, polyaniline/ZnO, and polyaniline/TiO_2 + ZnO, Polym. Compos. 35 (2014) 351–363.
[28] S. Joseph, J.C. McClure, R. Chianelli, P. Pich, P.J. Sebastian, Conducting polymer-coated stainless steel bipolar plates for proton exchange membrane fuel cells (PEMFC), Int. J. Hydrogen Energy 30 (2005) 1339–1344.
[29] D. Kowalski, M. Ueda, T. Ohtsuka, Corrosion protection of steel by bi-layered polypyrrole doped with molybdophosphate and naphthalenedisulfonate anions, Corros. Sci. 49 (2007) 1635–1644.
[30] J. Alam, U. Riaz, S. Ahmad, High performance corrosion resistant polyaniline/alkyde cofriendly coatings, Curr. Appl. Phys. 9 (2009) 80–86.
[31] A. Olad, H. Rasouli, Enhanced corrosion protective coating based on conducting polyaniline/zinc nanocomposite, J. Appl. Polym. Sci. 15 (2010) 2221–2227.
[32] M. Ates, T. Karazehir, F. Arican, N. Eren, Electrolyte type and concentration effects on poly(3-(2-aminoethyl thiophene) electrocoated on glassy carbon electrode via impedimetric study, Iran. Polym. J. 22 (2013) 199–208.
[33] E. Sezer, B. Ustamehmetoglu, A.S. Sarac, Chemical and electrochemical polymerization of pyrrole in the presence of N-substituted carbazoles, Synth. Met. 107 (1999) 7–17.
[34] L.M. Li, E.H. Liu, J. Li, Y.J. Yang, H.J. Shen, Z.Z. Huang, X.X. Xiang, W. Li, A doped activated carbon prepared from polyaniline for high performances supercapacitors, J. Power Sources 195 (2010) 1516–1521.
[35] J.G. Gonzalez-Rodriquez, M.A. Lucio-Garcia, M.E. Nicho, R. Cruz-Silva, M. Casales, E. Valenzuela, Improvement on the corrosion protection of conductive polymers in pemfc environments by adhesives, J. Power Sources 168 (2007) 184–190.
[36] Y.J. Ren, C.L. Zeng, Effect of conducting composite polypyrrole/polyaniline coatings on the corrosion resistance of type 304 stainless steel for bipolar plates of proton-exchange membrane fuel cells, J. Power Sources 182 (2008) 524–530.
[37] B. Duran, I. Çakmakci, G. Bereket, Role of supporting electrolyte on the corrosion performance of poly(carbazole) films deposited on stainless steel, Corros. Sci. 77 (2013) 194–201.